

## RESEARCH ARTICLE

10.1002/2015MS000492

## Key Points:

- Large inter-GCM variance for the projected future changes of surface fluxes
- Land surface models as a major source of the inter-GCM variance
- Enhancement of the intermodel variance through vegetation dynamics

## Correspondence to:

G. Wang,  
gwang@engr.uconn.edu

## Citation:

Yu, M., G. Wang, and H. Chen (2016), Quantifying the impacts of land surface schemes and dynamic vegetation on the model dependency of projected changes in surface energy and water budgets, *J. Adv. Model. Earth Syst.*, 8, 370–386, doi:10.1002/2015MS000492.

Received 3 JUN 2015

Accepted 20 FEB 2016

Accepted article online 25 FEB 2016

Published online 18 MAR 2016

## Quantifying the impacts of land surface schemes and dynamic vegetation on the model dependency of projected changes in surface energy and water budgets

Miao Yu<sup>1,2</sup>, Guiling Wang<sup>2</sup>, and Haishan Chen<sup>1</sup>

<sup>1</sup>Collaborative Innovation Center on Forecast and Evaluation of Meteorological Disasters/Key Laboratory of Meteorological Disaster of Ministry of Education, Nanjing University of Information Science and Technology, Nanjing, China, <sup>2</sup>Department of Civil and Environmental Engineering and Center for Environmental Sciences and Engineering, University of Connecticut, Storrs, Connecticut, USA

**Abstract** Assessing and quantifying the uncertainties in projected future changes of energy and water budgets over land surface are important steps toward improving our confidence in climate change projections. In this study, the contribution of land surface models to the inter-GCM variation of projected future changes in land surface energy and water fluxes are assessed based on output from 19 global climate models (GCMs) and offline Community Land Model version 4 (CLM4) simulations driven by meteorological forcing from the 19 GCMs. Similar offline simulations using CLM4 with its dynamic vegetation submodel are also conducted to investigate how dynamic vegetation feedback, a process that is being added to more earth system models, may amplify or moderate the intermodel variations of projected future changes. Projected changes are quantified as the difference between the 2081–2100 period from the Representative Concentration Pathway 8.5 (RCP8.5) future experiment and the 1981–2000 period from the historical simulation. Under RCP8.5, projected changes in surface water and heat fluxes show a high degree of model dependency across the globe. Although precipitation is very likely to increase in the high latitudes of the Northern Hemisphere, a high degree of model-related uncertainty exists for evapotranspiration, soil water content, and surface runoff, suggesting discrepancy among land surface models (LSMs) in simulating the surface hydrological processes and snow-related processes. Large model-related uncertainties for the surface water budget also exist in the Tropics including southeastern South America and Central Africa. These uncertainties would be reduced in the hypothetical scenario of a single near-perfect land surface model being used across all GCMs, suggesting the potential to reduce uncertainties through the use of more consistent approaches toward land surface model development. Under such a scenario, the most significant reduction is likely to be seen in the Northern Hemisphere high latitudes. Including representation of vegetation dynamics is expected to further amplify the model-related uncertainties in projected future changes in surface water and heat fluxes as well as soil moisture content. This is especially the case in the high latitudes of the Northern Hemisphere (e.g., northwestern North America and central North Asia) where the projected vegetation changes are uncertain and in the Tropics (e.g., the Amazon and Congo Basins) where dense vegetation exists. Findings from this study highlight the importance of improving land surface model parameterizations related to soil and snow processes, as well as the importance of improving the accuracy of dynamic vegetation models.

### 1. Introduction

© 2016. The Authors.

This is an open access article under the terms of the Creative Commons Attribution-NonCommercial-NoDerivs License, which permits use and distribution in any medium, provided the original work is properly cited, the use is non-commercial and no modifications or adaptations are made.

Climate change has become a major concern for societies and communities. The focus is not only on where and how severe the changes might be but also on its possible consequence for human and the environment. Based on model output from a large number of modeling experiments, the Intergovernmental Panel on Climate Change Fifth Assessment Report (IPCC AR5) [Collins et al., 2013] suggested that global mean surface temperature during the last 20 years of 21st century will “likely” exceed 2°C above 1850–1900 under a moderate greenhouse gas emission (GHG) scenario, the Representative Concentration Pathway (RCP) 6.0. This increment will be “very likely” under a high GHG scenario, RCP8.5. The warming trend over land is “very likely” more severe than that over ocean. Global precipitation is projected to increase by 1–3% °C<sup>-1</sup> at the end of the 21st century with substantial spatial variation, accompanied by changes in surface humidity,

evapotranspiration, soil water content, and surface runoff [Barnett *et al.*, 2008; Dai, 2013; Hua *et al.*, 2013; O'Gorman and Muller, 2010].

The trend and magnitude of projected future changes are subject to a large degree of uncertainties, for which the differences between model structures are considered to be one of the major sources [Knutti *et al.*, 2010; Murphy *et al.*, 2004]. The other two major sources of uncertainties are the different anthropogenic emissions scenarios which depends on socioeconomic factors [Moss *et al.*, 2010], and the chaotic and nonlinear nature of climate system itself [Deser *et al.*, 2012; Hawkins and Sutton, 2009, 2011]. Uncertainty, any departure from a realistic state of a complex system, has been commonly estimated by climate scientists based on the consistency and spread of projections among model results in the IPCC AR5. Although there are major improvements since IPCC AR4 regarding model parameterization and availability of long period of observations for validating model performances, uncertainties have not become smaller [Knutti and Sedláček, 2013]. Furthermore, inclusion of other physical or dynamical mechanisms in the earth system models adds additional uncertainties. The major advancement of the incorporation of carbon-climate interactions introduces several parameters representing terrestrial biogeochemical and biogeophysical processes. Values for many of these parameters are very uncertain due to the limited observations for validations. The uncertainties about carbon storage and fluxes in observations and simulations have been evaluated in a large number of studies at the regional and global scales [Ahlström *et al.*, 2013; Friedlingstein *et al.*, 2006; Piao *et al.*, 2012; Shao *et al.*, 2013]. How to minimize the uncertainty for climate projections based on multiple models is a challenging task [Knutti *et al.*, 2010].

LSMs are important components in the earth system models (ESMs) or GCMs. They simulate turbulent transport of energy, mass, and momentum between land and the overlying atmosphere. As the surface fluxes and their changes play important roles in shaping the triggering mechanisms of convective precipitation, accurate representation of land surface processes therefore realistic estimate of surface fluxes are critical for climate modeling and predictions. However, major uncertainties exist, as reflected by the large differences among output from different LSMs driven by the same atmospheric forcing [Liang and Guo, 2003; Pitman and Henderson-Sellers, 1998; Wood *et al.*, 1998]. When these LSMs are coupled to atmospheric models as the land component of the ESMs or GCMs, the intermodel differences from the land component and those from other components together shape the intermodel differences or model-related uncertainties in the predictions from ESMs or GCMs.

Among processes over land, modeling of the dynamic vegetation feedback is of great importance since vegetation is a key factor controlling land-atmosphere flux exchanges through its impact on surface albedo, evapotranspiration, and surface roughness [Bonan, 2008]. Both present-day climate simulation and future climate projections can be affected by the dynamic vegetation feedback [e.g., Martin and Levine 2012; Yu *et al.* 2015]. Different LSMs vary significantly in the representation of vegetation and vegetation dynamics, and achieve different levels of success in simulating the spatial and temporal variability of vegetation [Murray-Tortarolo *et al.*, 2013]. In models with prescribed vegetation, the fractional coverage of different vegetation types is specified according to satellite data; some models specify the leaf area index (LAI) and its seasonal cycle based on satellite data while others utilize a predictive phenology scheme. In models with dynamic vegetation, both the vegetation demography and structure will be predicted by the model, and plant phenology that determines the LAI seasonal cycle is prognostic based on carbon budget in some models and based on hydrometeorological thresholds in others. While the dynamic vegetation models represent a desirable model capacity especially in the context of future predictions, they cause additional uncertainties in simulating surface heat and water fluxes. As vegetation responds to changes in the climate, the resulting vegetation changes will then feedback to further influence the regional climate. Therefore, vegetation dynamics has the potential to amplify biases and intermodel differences in the model physical climate [Wang *et al.*, 2015]. Moreover, only several of the GCMs participating in the IPCC AR5 include representation of vegetation dynamics. The uncertainty in the carbon cycles could be mixed together with the uncertainty of vegetation model parameterization, making it very difficult to distinguish them in their effects on uncertainty of climate changes [Higgins and Harte, 2012; Jiang *et al.*, 2012].

In this study, we try to quantify the uncertainties in GCM-projected surface fluxes changes that may be caused by different LSMs based on output from 19 CMIP5 GCMs/ESMs [Taylor *et al.* 2012] and on results from a group of experiments using one LSM driven with atmospheric forcings from the 19 GCMs/ESMs. We focus on assessing the uncertainty of simulated future changes in land surface water and energy fluxes, as

these fluxes influence regional climate and shape climate impacts. The high GHG concentration scenario (RCP8.5) is chosen as an example. Moreover, as dynamic vegetation is being added to more and more GCMs/ESMs, its impact on the model-related uncertainties is also investigated here, based on an additional group of experiments that include dynamic vegetation modeling. In the rest of the paper, the experimental design and methodology are described in section 2, and results are analyzed in section 3. A discussion is supplied in section 4; conclusions and summaries are in section 5.

## 2. Model, Methodology, and Experimental Design

### 2.1. Land Surface Model

The LSM used in this study is the CLM4 [Lawrence *et al.*, 2011; Oleson *et al.*, 2010] with modifications to the gross primary production (GPP) parameterization and to the phenology schemes for tropical broadleaf drought deciduous trees and evergreen trees [Wang *et al.*, 2015; Yu *et al.*, 2014]. The CLM4 is a submodel of the Community Earth System Model version 1.0.4 (CESM 1.0.4) of the National Center for Atmospheric Research (NCAR), depicting the mass, momentum, and energy transport between land and atmosphere. The land surface in each grid cell of the model is represented as a combination of five land cover types including glacier, lake, wetland, urban, and vegetated. The vegetated portion of each grid cell can contain bare soil, up to two crop types, and up to 15 unmanaged plant functional types (PFTs) including trees, grasses, and shrubs. The version used here is exactly the same as the one in Yu *et al.* [2014] and Wang *et al.* [2015].

In quantifying vegetation, CLM4 supports three options. One uses satellite leaf area index data derived from Moderate Resolution Imaging Spectroradiometer (MODIS) to prescribe static vegetation cover in each month. Another uses a prognostic carbon-nitrogen model (CN) [Thornton and Rosenbloom, 2005; Thornton *et al.*, 2002] to model seasonal variation of vegetation structure with a prescribed vegetation demography. Specifically, under a given PFT distribution, CN simulates carbon fluxes (including photosynthesis and respiration) and updates carbon storage (therefore vegetation structure such as LAI) based on the resulting carbon budget. The third option uses the CN model combined with a dynamic vegetation model (DV) [Levis *et al.*, 2004] to simulate the vegetation demography and structure changes. The DV model simulates the annual biogeographic processes including competition, establishment, and survival based on the carbon-nitrogen budgets derived from the CN model. With the CN and DV (CNDV) model activated, CLM4 is capable of simulating the vegetation dynamics in response of climate change, and can capture the distribution of plant function types and their spatial variability reasonable well [Gotangco Castillo *et al.*, 2012; Mao *et al.*, 2012; Yu *et al.*, 2014].

### 2.2. Experimental Design

In this study, the surface meteorological forcing to drive CLM4 and CLM4-CNDV were derived from output of Global Climate Models (GCMs) participating in the CMIP5, including incident solar radiation, precipitation, temperature, pressure, humidity, and wind. Based on the availability of the 3 or 6 hourly output for the six forcing variables, 19 GCMs (Table 1) were selected. The RCP8.5 is chosen to maximize the signal for projected changes. The atmospheric CO<sub>2</sub> concentration is prescribed in CLM4 and CLM4-CNDV experiments according to the CO<sub>2</sub> level in the 19 GCMs RCP8.5 simulations.

Among the 19 GCMs selected in this study, only 10 of them contain a dynamic vegetation model, such as the AVIM2 in the BCC family models, the LM3V in the GFDL family models, and the SEIB-DGVM in the MIROC-ESM family models. Others prescribe vegetation distribution and structure based on observational data. For describing future change of land use, some of the GCMs (e.g., the GFDL family models and IPSL-CM5A-LR) include prescribed land cover changes based on the data set of Hurtt *et al.* [2006, 2011].

Two groups of experiments were conducted in this study. One group runs CLM4 with prescribed satellite phenology (referred to as SP experiments), and the other runs CLM4 with the dynamic vegetation model CNDV (referred to as DV experiments). Each group includes 19 pairs, with each pair forced by 3 or 6 hourly output from one of the 19 GCMs throughout a corresponding 20 year period: 1981–2000 for a present-day simulation and 2081–2100 for a future simulation. Each SP experiment is a cycle run of 80 years and each DV experiment is a cycle run of 200 years to derive the corresponding quasiequilibrium state. The NCAR provided CN initial states, which was derived from a long spin-up simulation under present day climate

**Table 1.** Models Specification

Model name	LSMs	Dynamic Vegetation	Original Resolution (lon × lat)	References
ACCESS1.0	MOSES2.2 [Martin <i>et al.</i> , 2006]	No	145 × 192	Bi <i>et al.</i> [2013]
BCC-CSM1.1	BCC_AVIM1.0	AVIM2 [Ji, 1995; Ji <i>et al.</i> , 2008]	64 × 128	Wu <i>et al.</i> [2013]
BCC-CSM1.1(m)	BCC_AVIM1.0	AVIM2	160 × 320	Wu <i>et al.</i> [2014]
BNU-ESM	CoLM	BNUDGVM (LPJ-DyN)	64 × 128	Ji <i>et al.</i> [2014]
CCSM4	CLM3.5 [Oleson <i>et al.</i> , 2008; Stockli <i>et al.</i> , 2008]	DGVM	192 × 288	Gent <i>et al.</i> [2011]
CMCC-CM	SILVA [Alessandri <i>et al.</i> , 2012]	No	240 × 480	Bellucci <i>et al.</i> [2013]
CNRM-CM5	SURFEX-TRIP	No	128 × 256	Volodire <i>et al.</i> [2013]
FGOALS-g2	CLM3	No	60 × 128	Li <i>et al.</i> [2013]
GFDL-CM3	LM3 [Donner <i>et al.</i> , 2011]	LM3V [Shevliakova <i>et al.</i> , 2009]	90 × 144	Griffies <i>et al.</i> [2011]
GFDL-ESM2G	LM3	LM3V	90 × 144	Dunne <i>et al.</i> [2012]
GFDL-ESM2M	LM3	LM3V	90 × 144	Dunne <i>et al.</i> [2012]
HadGEM2-ES	JULES (from MOSES2) +TRIFFID	TRIFFID [Cox, 2001]	144 × 192	Collins <i>et al.</i> [2011]
INM-CM4	Simple model [Volodin and Lykosov, 1998]	No	120 × 180	Volodin <i>et al.</i> [2010]
IPSL-CM5A-LR	ORCHIDEE	No	96 × 96	Dufresne <i>et al.</i> [2013]
IPSL-CM5A-MR	ORCHIDEE	No	143 × 144	Dufresne <i>et al.</i> [2013]
MIROC5	MATSIRO [Takata <i>et al.</i> , 2003]	No	128 × 256	Watanabe <i>et al.</i> [2010]
MIROC-ESM	MATSIRO+SEIB-DGVM	SEIB-DGVM	64 × 128	Watanabe <i>et al.</i> [2011]
MIROC-ESM-CHEM	MATSIRO+SEIB-DGVM	SEIB-DGVM	64 × 128	Watanabe <i>et al.</i> [2011]
MRI-CGCM3	HAL [Hosaka <i>et al.</i> , 2011]	No	160 × 320	Yukimoto <i>et al.</i> [2012]

forcing [Thornton and Rosenbloom, 2005; Thornton *et al.*, 2007], were used as the initial carbon and nitrogen storage. The initial vegetation cover for the DV experiments was bare ground. The CO<sub>2</sub> concentrations were set according to the 1981–2000 observational and 2081–2100 RCP8.5 levels. The last 20 years of each simulation are used for the analysis here. Quantitatively, results from this cycling approach based on 20 years of future climate are comparable to what would be derived from a continuous transient simulation [Yu *et al.*, 2014].

Monthly output from the CMIP5 GCMs for the present and future 20 years for sensible heat fluxes, evapotranspiration (ET), soil water in the top 10 cm, and surface runoff are used as the reference for comparison. However, not all variables are available from all 19 GCMs. The CMCC-CM and HadGEM-ES models do not have surface runoff in their output and were therefore excluded from the analysis of this variable; Likewise, CMCC-CM and CNRM-CM5 were excluded from the analysis on soil water in the top 10 cm. In addition, the BNU-ESM output for soil water content is for the top 20 cm and FGOALS-g2 for the top 9 cm, and they were scaled linearly to derive the approximately value for the top 10cm.

The surface fluxes and states from a GCM and from the corresponding SP and DV simulations share the same meteorological forcing. In the 19 SP experiments, the land-atmosphere flux exchanges are solved by the same LSM that assumes the same static vegetation distribution; the DV experiments are otherwise the same as the SP experiments except that the land surface model also simulates dynamic vegetation distribution. Therefore, the difference between the intermodel variations derived from the 19 GCMs and the 19 SP experiments are indicative of the uncertainty due to the use of different LSMs, while comparison between the SP and DV simulations sheds light on how including dynamic vegetation may influence the model-related uncertainty.

### 2.3. Quantifying the Uncertainty and Its Sources

Two different methods are used here to assess the model uncertainty in each specific group of simulations (GCM, SP, or DV). One is the model agreement regarding the projected future changes based on the number of models agreeing on the sign of changes, which is adopted from previous studies [Wang, 2005; IPCC AR4, 2007]. The other is the intermodel standard deviation (IMSD) for the projected changes in meteorological forcing and in water and energy fluxes to quantify the spread or uncertainty across models. Since the land surface in each SP experiment shares the same meteorological forcing as that in the corresponding GCM, the difference in the IMSD of simulated future changes of land surface variables between GCMs and the SP experiments reflect the potential contribution of using different LSMs to the intermodel

uncertainties, or the extent to which the IMSD could be potentially reduced if a single LSM were to be used across all GCMs:

$$\text{Contribution of LSMs} = 1 - \frac{\sigma_{\text{SP}}^2}{\sigma_{\text{GCM}}^2} \quad (1)$$

where  $\sigma_{\text{GCM}}^2$  is the variance of future change for a specific variable in water and energy fluxes derived from the GCMs;  $\sigma_{\text{SP}}^2$  is the variance derived from the SP experiments. Values for the contribution of LSMs are typically between 0 and 1, and negative values are possible due to noises.

The amplification effect due to dynamic vegetation on the intermodel uncertainties can be assessed through the ratio of intermodel variance of the flux changes between the DV and SP experiments:

$$\text{Amplification by DV} = \frac{\sigma_{\text{DV}}^2}{\sigma_{\text{SP}}^2} \quad (2)$$

where  $\sigma_{\text{DV}}^2$  is the intermodel variance of flux changes derived from the DV experiments.

#### 2.4. Caveats and Potential Impacts

The experimental design and the approaches to quantifying the model uncertainties and land surface contribution are subject to two limitations that could complicate the interpretation of the model results. The first has to do with the role of internal climate variability. The spread of projected changes in the CMIP5 model outputs results from not only differences in model formulation but also internal climate variability. The unforced climate variability has effects on climate change projections, particularly at the regional spatial scale [Hawkins and Sutton, 2009, 2011].  $\sigma_{\text{GCM}}^2$  is therefore not entirely a reflection of model-related uncertainty. However, since internal climate variability is also present in the meteorological forcing for the offline CLM experiments, its impact on the ratio of  $\sigma_{\text{SP}}^2$  to  $\sigma_{\text{GCM}}^2$  may partially cancel out. Moreover, given the long lead time considered here, the contribution from internal variability is typically much smaller than that from model uncertainty. As an example, Figure 1 shows the standard deviation of the projected future changes in surface variables of concern to this study, derived from a 30 member ensemble from the Community Earth System Model Large Ensemble (CESM-LE) project [Kay et al., 2014]. Different ensemble members slightly differ in their initial conditions on 1 January 1920 and all include the CMIP5 historical run (1920–2005) and RCP8.5 run (2006–2100). The magnitudes of future changes derived from the CESM-LE experiments are comparable with those from our experiments, yet the spread due to internal climate variability as shown in Figure 1 is much smaller than the intermodel spread (as presented in section 3). The contribution of internal variability to the intermodel standard deviation can therefore be neglected, and equation (1) provides an approximately valid metric indicative of the potential contribution of LSMs to the GCMs model uncertainty.

The other limitation has to do with the lack of feedback from the land surface to the driving atmospheric variables in the SP experiments used to diagnose uncertainties that would remain in a hypothetical scenario where a single LSM was used across all GCMs. The projected future changes of surface fluxes from the SP experiments are likely to differ from what might have been obtained if we were to rerun each of the CMIP5 coupled models in a “transplant” mode with the original land surface scheme replaced by CLM4. The extent to which they do differ will depend on how strongly each variable is affected by surface-to-atmosphere coupling. Of all the variables analyzed in this study, sensible heat flux is likely to be the most sensitive to the lack of coupling: as the surface temperature is allowed to change but the atmospheric temperatures are not allowed to respond in the SP experiments, the magnitude of sensible heat fluxes might be overestimated. However, this effect will be present in the SP simulations corresponding to all GCMs, and for both the past and future periods. It is likely that at least part of its potential effect will be cancelled in the estimate of land surface contribution to the intermodel uncertainty, but it is difficult to quantify and will remain a complicating factor.

### 3. Results

In this study, our analysis focuses primarily on the intermodel spread of the annual average of future changes as the main signal of interest, and assesses the contribution from land surface models to this

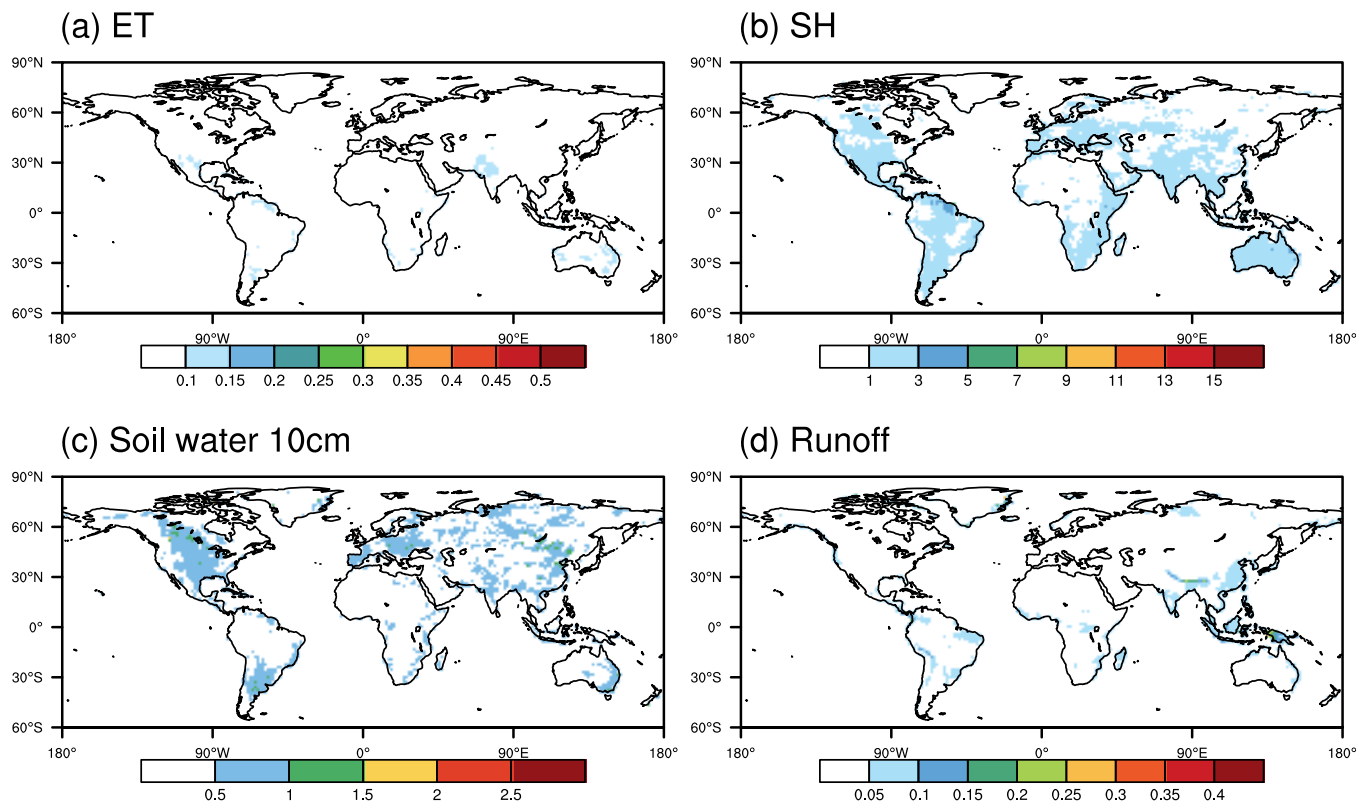


**Figure 1.** The standard deviations of the future changes in 2081–2100 relative to 1981–2000 under RCP8.5 in annual means of ET (a, unit: mm/d), sensible heat flux(b, unit: W/m<sup>2</sup>), soil water in top 10 cm (c, unit: kg/m<sup>2</sup>), and runoff (d, unit: mm/d) from the 30 member of CESM-LE ensemble. The color scales are set as the same as those in Figures 4, 6, 8, and 10, respectively, to compare the IMSD for each variable.

spread and how including vegetation dynamics might influence the intermodel spread. For each variable analyzed in this study, both the projected future changes and the intermodel standard deviation show a high degree of seasonality that is dominated by the seasonality of the variable itself. However, the metrics we use to quantify the impact of land surface models and vegetation dynamics on the model-related uncertainty (equations (1) and (2)) show very little variation from season to season, and the spatial pattern and magnitude are very similar to the results based on the annual averages.

### 3.1. Meteorological Forcings

Figure 2 shows the future changes of surface temperature, precipitation, and solar radiation in 2081–2100 with respect to 1981–2000 projected by the 19 GCMs and their intermodel uncertainties. These GCMs agree on a warming trend that is stronger in the Northern Hemisphere than in the Southern Hemisphere. The area north of about 60°N is projected to experience the strongest warming which is likely to be larger than 6°C. The IMSD is large in northeastern North America and northeastern Asia in the high latitudes, over the Tibetan Plateau in the middle latitudes, and over Amazon in the Tropics. The areas with high IMSD correspond well with the areas with strong warming except the northern Eurasia. Large IMSD in the high latitudes and the Tibetan Plateau may be related to the difficulty of simulating snow-related processes.

Future precipitation is projected to decrease in southwestern North America, the Amazon, northern and southwestern South America, areas around the Mediterranean, and South Africa, and increase in the region north of about 50°N, East and South Asia, and Central and East Africa. These changes are mostly accompanied with the opposite changes of surface downward solar radiation since cloudiness is likely to increase with precipitation. The exceptions where both solar radiation and precipitation are projected to increase include the eastern USA, western edge of South America, Central Europe, and southeastern China. Agreement on the precipitation change is high in the high latitudes north of about 50°N, around the Mediterranean, in South Asia, and East and South Africa. The model spread is large in the Tropics, mostly attributed to the high intermodel uncertainty in the Amazon and the maritime continent.

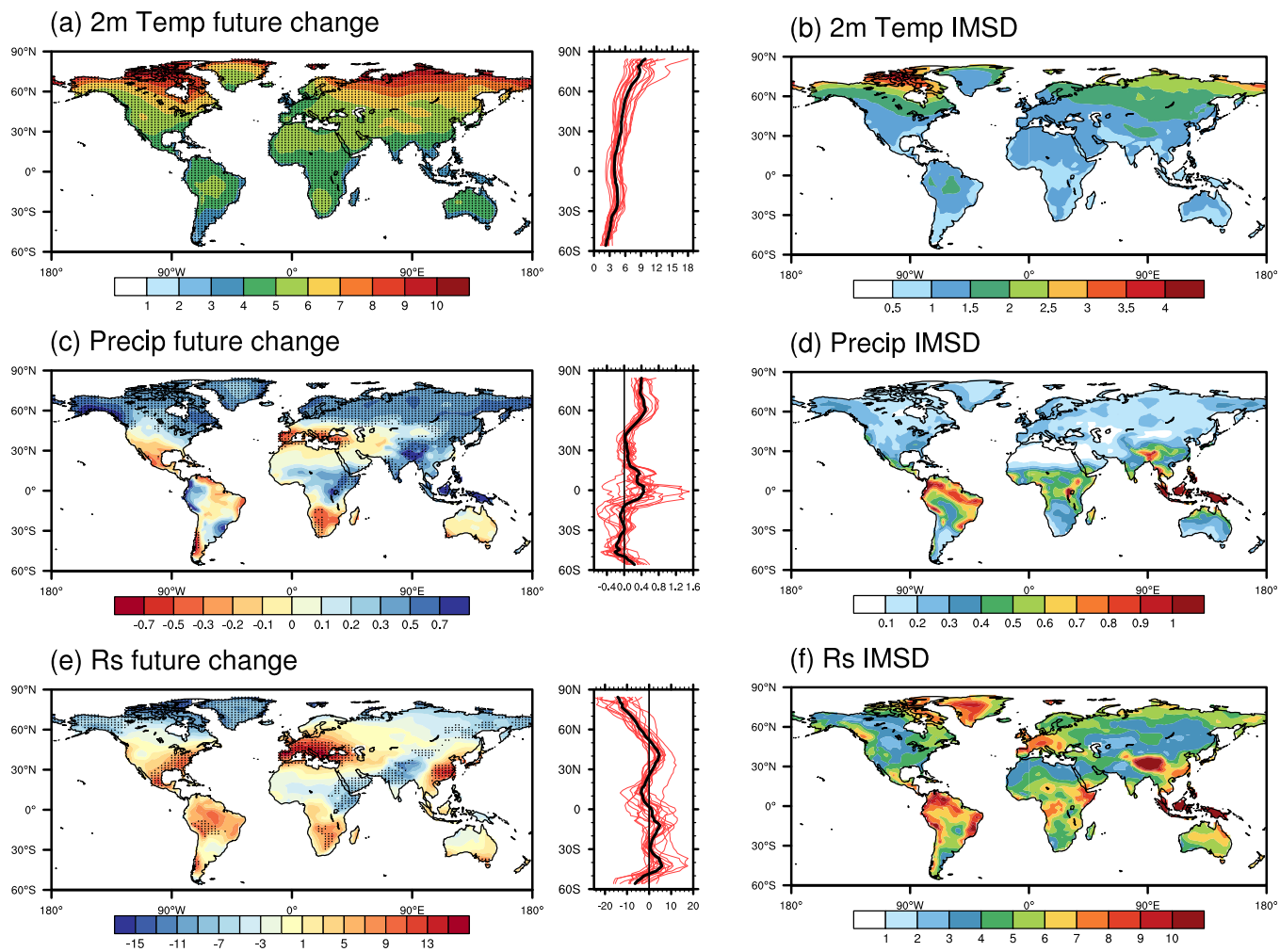


**Figure 2.** Future change patterns in 2081–2100 relative to 1981–2000 under RCP8.5 for annual means of 2 m temperature (top row, unit: K), precipitation (middle row, unit: mm/d), and surface downward shortwave solar radiation (bottom row, unit: W/m<sup>2</sup>), with their zonal averages showing on the right (a, c, e). Right column shows their IMSD (b, d, f). Stippling means all the 19 models agree on the warming trend, or 17/19 models agree on the projected direction of precipitation or downward solar radiation. The red lines show future changes from different GCMs and the black line is their average.

Correspondingly, large IMSD for future change of downward solar radiation is found in the Amazon, Central and East Africa, the Tibetan Plateau, and the maritime continent, where the large IMSD of future change in precipitation may suggest a role of cloud feedback in explaining the model uncertainties of solar radiation changes. The IMSD for solar radiation is also large in the high latitudes including the Greenland Island, northwestern North America and South Europe.

### 3.2. Future Changes of Vegetation

The projected future climate changes are expected to cause significant changes in vegetation distribution, structure, and functions. Details about the projected future vegetation changes can be found in Yu *et al.* [2014]. Here we only focus on change of vegetation density as represented by leaf area index (LAI, defined as the total one-sided leaf area per unit area of ground), as LAI is a key variable controlling the water and energy flux exchanges between land surface and the atmosphere thus controlling the surface water and energy budget. The Global Inventory Monitoring and Modeling Studies (GIMMS) [Tucker *et al.*, 2005; Zhou *et al.*, 2001] data set from July 1981 to December 2000 is used to evaluate the model performance in simulating the vegetation dynamics. The ensemble DV experiments generally capture the spatial pattern of JJA and DJF LAI well (Figures 3a–3d); exceptions include underestimation of LAI in the boreal region and overestimation in the Amazon. The overestimation in the tropical areas is likely to be exaggerated considering

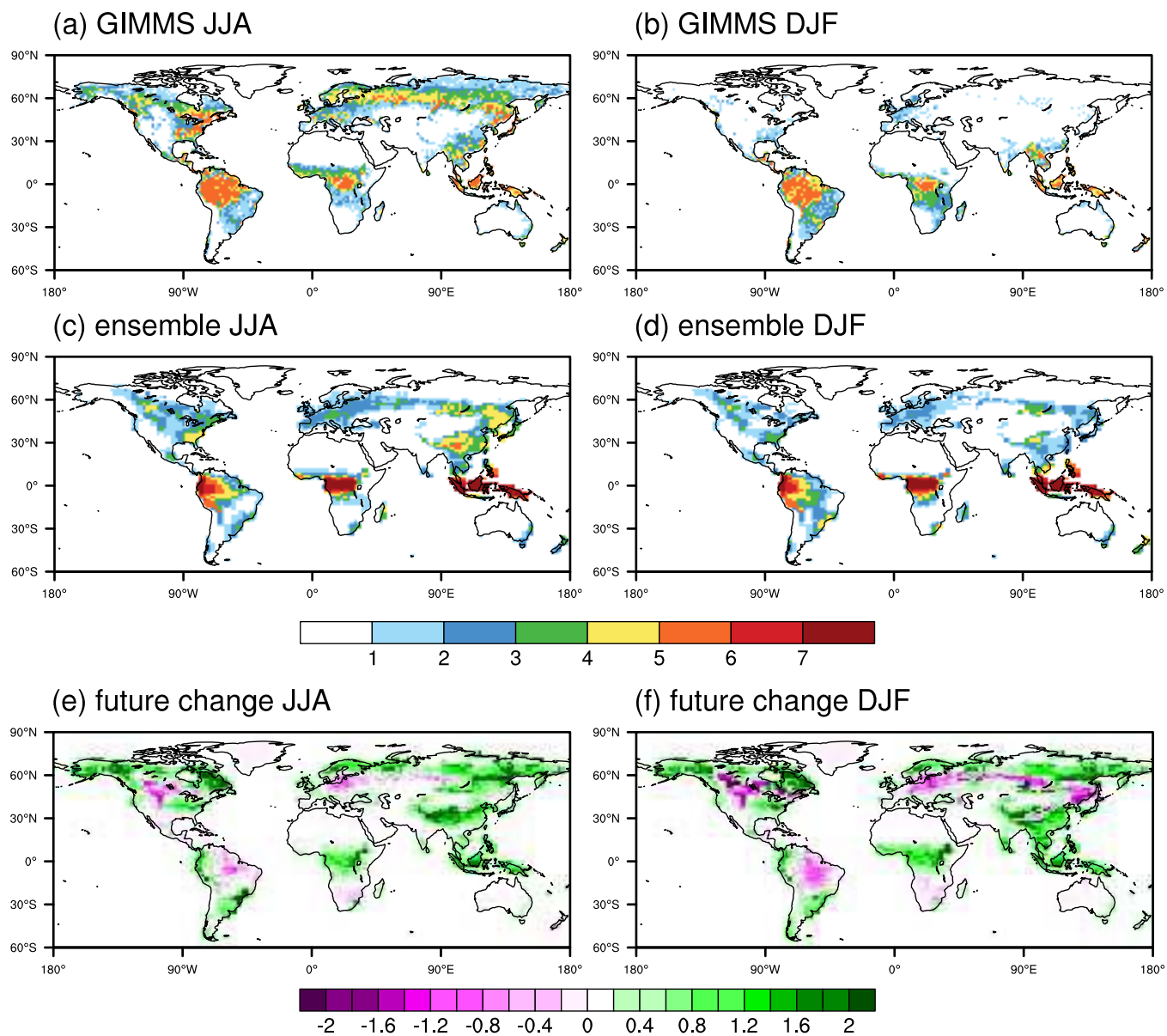


**Figure 3.** JJA (left column, in 1982–2000) and DJF (right column, in 1981–1999) LAI derived from the observation (a, b), the ensemble DV experiments (c, d), and their future changes under RCP8.5 as of 2082–2100 and 2081–2099, respectively (e, f).

the existence of negative bias in satellite-based LAI relative to in situ data set over densely vegetated areas [Roberts *et al.*, 1996].

The ensemble mean of the DV experiments projects a decrease of vegetation density in Central North America, the Amazon, Central Europe, areas around 50–60°N of Central Asia, northeastern and Central China, and South Africa. Vegetation is likely to grow denser in the high latitudes of North America and Eurasia, and in Central Africa and South Asia (Figure 4a). This pattern is found in both JJA and DJF but the magnitude of decrease in DJF is larger than that in JJA particularly in northeastern China (Figures 3e and 3f). It is found in Yu *et al.* [2014] that CO<sub>2</sub> fertilization is the primary cause for the projected increase of tree and shrub coverage that underlies the increase of LAI. Trees are projected to be replaced by grasses in most of the temperate areas where LAI is projected to decrease. However in the Amazon and South Africa, the decrease of precipitation is the main cause for the LAI decrease. Projections for LAI changes show relatively high IMSD in northwestern and northeastern North America, 50–60°N of Eurasia, northern South America,

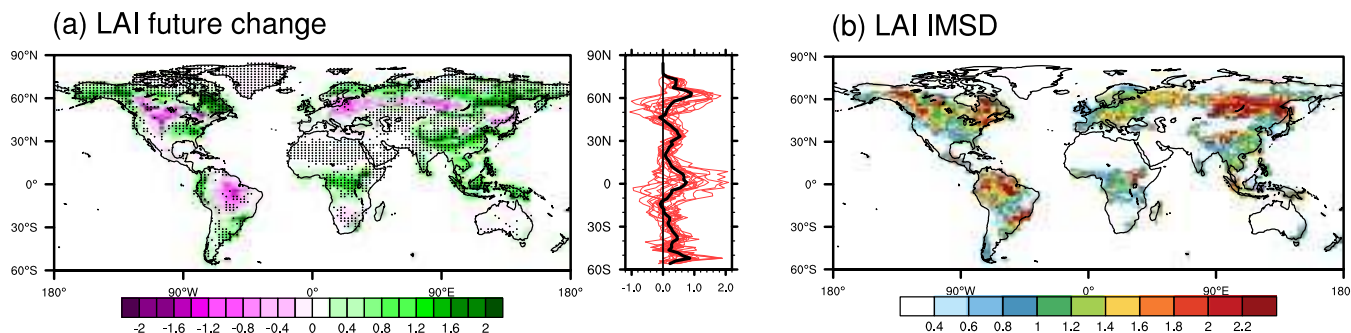


**Figure 4.** Future change of annual LAI in 2081–2100 relative to 1981–2000 under RCP8.5 with the zonal average showing on the right (a) and its IMSD (b). Stippling means 15/19 models agree on change directions. The lines in the zonal average plot mean the results from different GCMs and the average.

East Africa, and the Tibetan Plateau. The model spread for zonal-averaged LAI projections is larger in the Tropics and in areas between 50 and 60°N than the other latitudes (Figure 4b).

### 3.3. Future Changes in Surface Energy and Water Budgets

Annual ET is projected to increase over most of the global landmass by the GCMs. However, in southern North America, South Africa, the Amazon, and the Mediterranean area, ET is projected to decrease by all three sets of experiments, due to drying trends in these regions. There is a high degree of agreement among the 19 models on the decrease of ET in South Africa and the Mediterranean areas. In the northern high latitudes, the SP and DV experiments produce little systematic changes in the northern high latitudes while the GCMs produce large increase of ET there (Figure 5), and the corresponding IMSD is low for all three sets of experiments. In all three sets of experiments, the IMSD is large in northern South America, East Africa, and northeastern Australia. The IMSD is relatively large among GCMs in Central North America, South Europe, 50–60°N of Central Asia and area over the Tibetan Plateau. Results in Figure 6a suggest that LSMs are likely to be responsible for a large fraction of the IMSD of ET among the GCMs in areas north of about 40°N, the Amazon, Sahel and areas around the Congo basin (Figure 6a). Incorporation of dynamic vegetation is found to increase the IMSD in northwestern North America, areas around 60°N of Asia, The Tibetan Plateau, the Amazon, and areas north and south of the Congo basin (Figure 6b).

Future changes of sensible heat fluxes are projected to increase across the globe, with a high degree of agreement among the models in areas where simulated precipitation and ET decrease, including southern North America, the Amazon, South Africa, and the Mediterranean areas. Strong increase of sensible heat fluxes in southeastern China is also produced with a high degree of model agreement in all three sets of simulations (Figure 7), although ET in this region is projected to increase. The simultaneous increase of ET and sensible heat flux reflects an increase of net radiation. The GCMs show large IMSD of sensible heat flux changes in northeastern South America, East Africa, southern edge of Tibetan Plateau and area among about 50–70°N of central Asia (Figure 7b). The intermodel spread is narrowed over most of these regions in the SP experiments (Figure 7d). While the lack of coupling in the SP and DV experiments influences the results for all variables, it is especially problematic for sensible heat flux. In the coupled GCMs, sensible heat flux provides a strong negative feedback on surface-to-boundary layer temperature gradient. For example, if large sensible heat fluxes develop due to changes in surface temperature, the atmospheric temperature (therefore vertical temperature gradient) in GCMs would adjust in response. This feedback mechanism is lacking in the offline experiments, which can lead to exaggerated changes of sensible heat flux in the offline ensembles. This is a possible reason for the large disparity of predicted sensible heat flux changes between the GCMs and the SP experiments in (Figures 7a and 7c). Our results indicate that different LSMs contribute to intermodel uncertainties for future changes of sensible heat fluxes mainly in Central North America, 50–70°N of Central Asia, the Amazon, and area north of Sahara in Africa (Figure 8a). Including dynamic vegetation further increases the magnitude of future changes in sensible heat fluxes; it also amplifies the IMSD in regions where large model spread in future change of vegetation is produced, including 50–70°N of Central and East Asia and the Amazon, and in regions where large spread of precipitation changes are simulated,

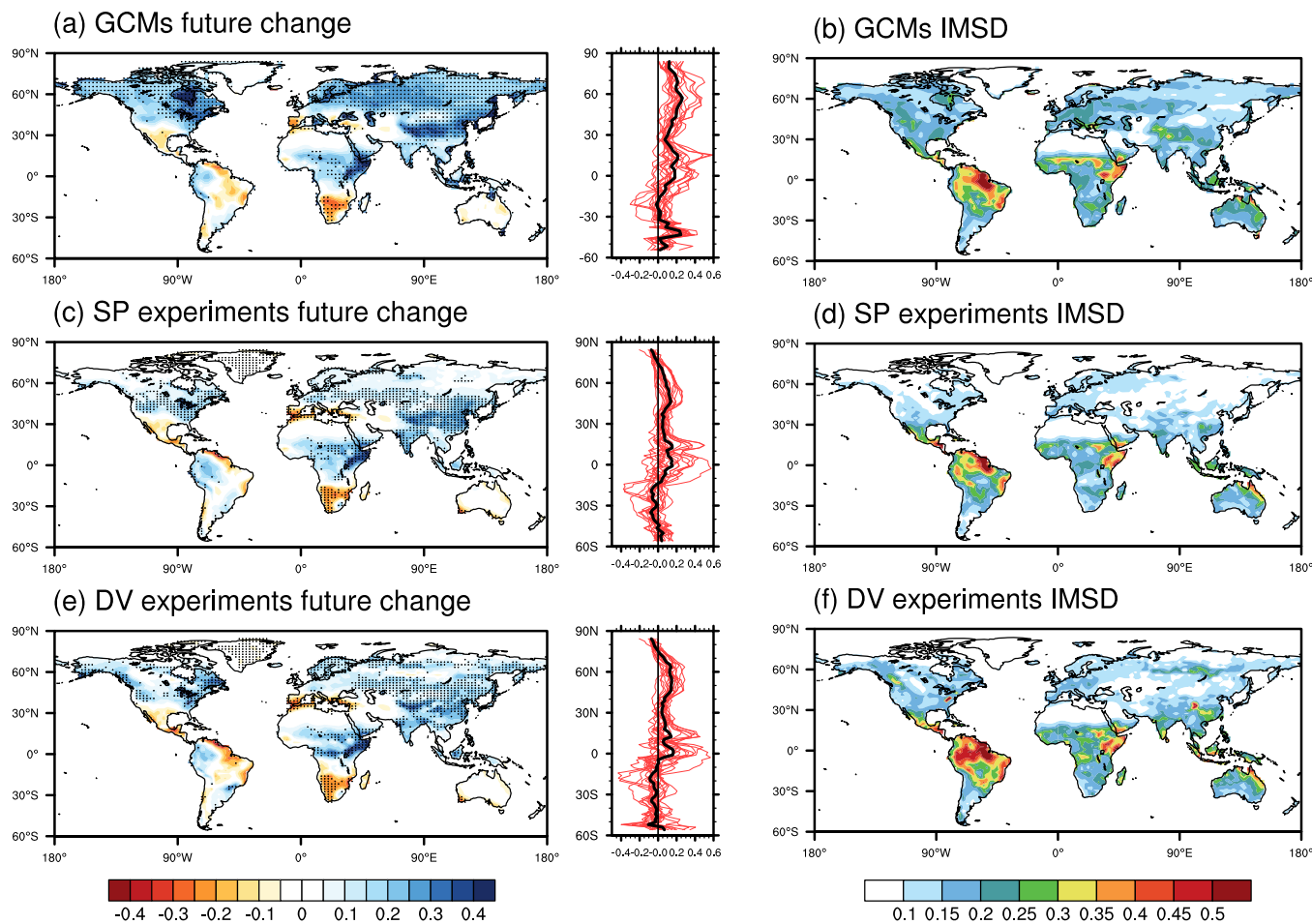


**Figure 5.** Future change of annual ET (unit: mm/day) in 2081–2100 relative to 1981–2000 under RCP8.5 simulated by the GCMs (top row), experiments SP (middle row), and experiments DV (bottom row) with their zonal average showing on the right (a, c, e). Stippling means 17/19 models agree on the signs of changes. The red lines show future changes from different simulations and the black line shows their average. Right column shows the IMSD (b, d, f).

including areas north and south of the Congo basin (Figure 8b). The increased model spread over the Tibetan Plateau is probably due to the combined uncertainties in downward solar radiation and vegetation.

The GCMs and the SP and DV experiments all produce drier soil in southern North America, the Amazon, South Africa, area around the Mediterranean, southeastern China, and Australia, likely due to the simulated decrease of precipitation there. In the northern high latitudes, including eastern Canada, Europe, and

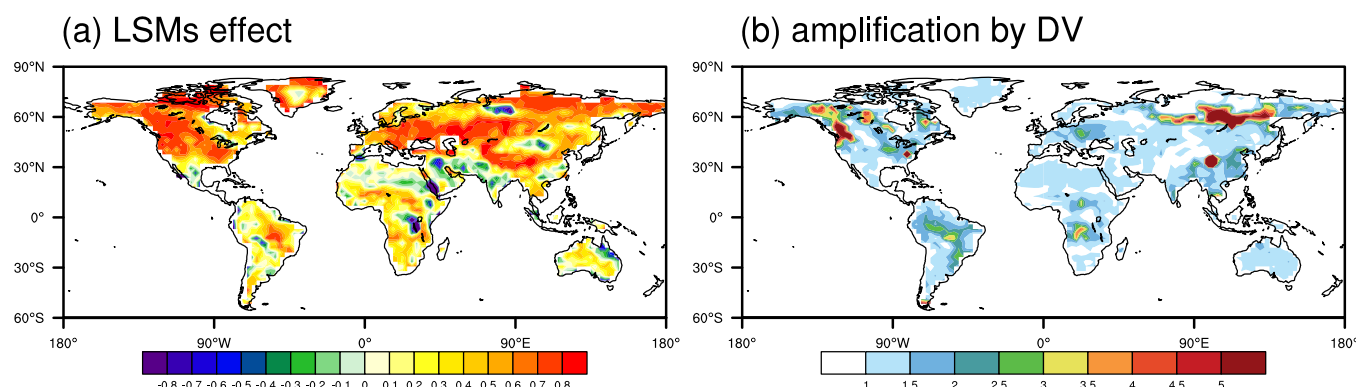


**Figure 6.** (a) Contribution effect of different LSMs on the inter-model uncertainties of annual ET and (b) the amplification effect due to dynamic vegetation.

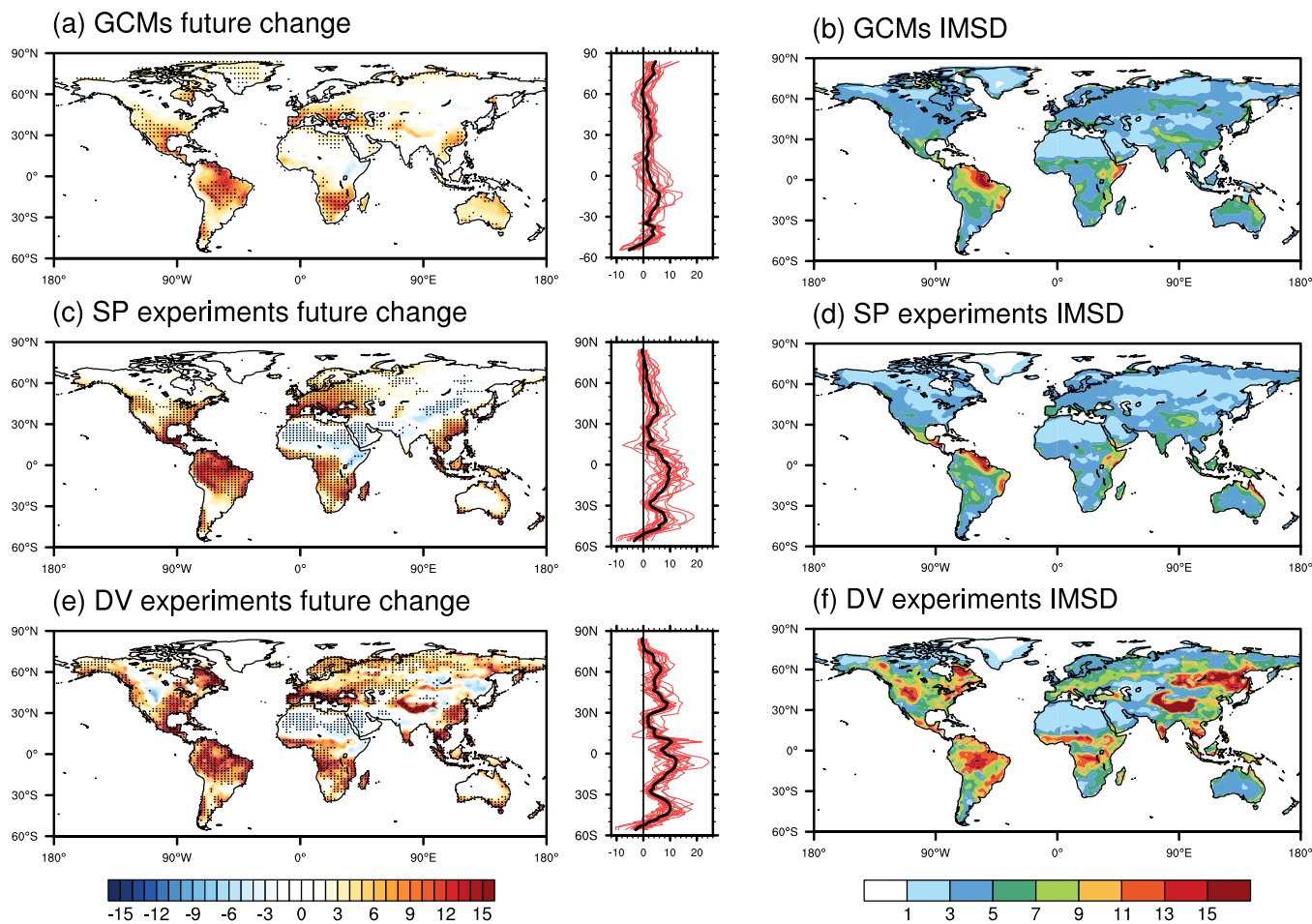


**Figure 7.** Similar as Figure 5, but for sensible heat fluxes (unit:  $\text{W}/\text{m}^2$ ).

eastern North Asia, the SP and DV experiments produce a trend that is opposite of that from the GCMs. This result can be specific to the land surface model used in this study, the CLM4. The future changes produced by CCSM4 (figure not shown), which uses an earlier version of CLM as its land component, are similar to future changes from the SP and DV experiments. The intermodel uncertainty for the soil water in top 10 cm is very high in the region north of about 50°N (Figure 9). Several GCMs produce very large magnitude of decrease there. The LSMs difference is likely to account for most of the model spread in the northern high latitudes and the Tibetan Plateau, suggesting a potentially high degree of inconsistency among LSMs in

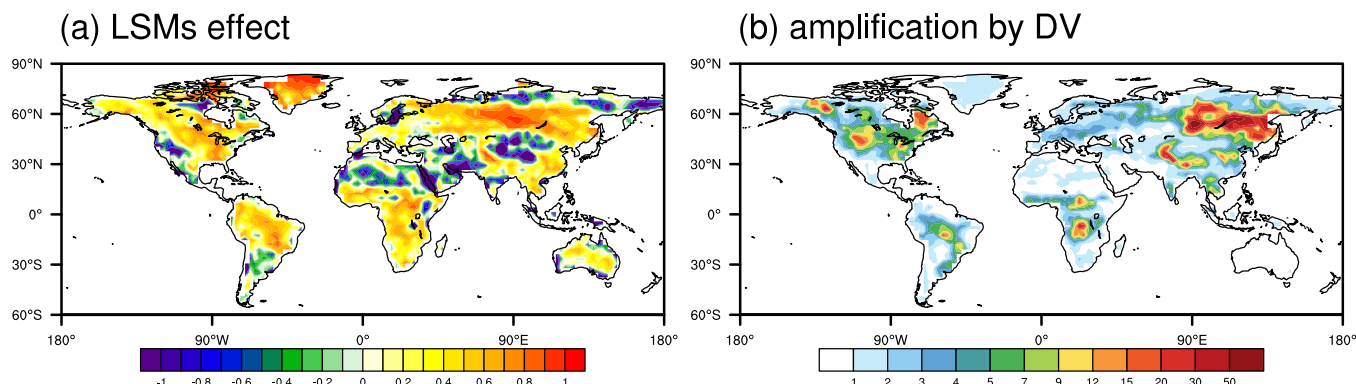


**Figure 8.** Similar as Figure 6, but for sensible heat fluxes.

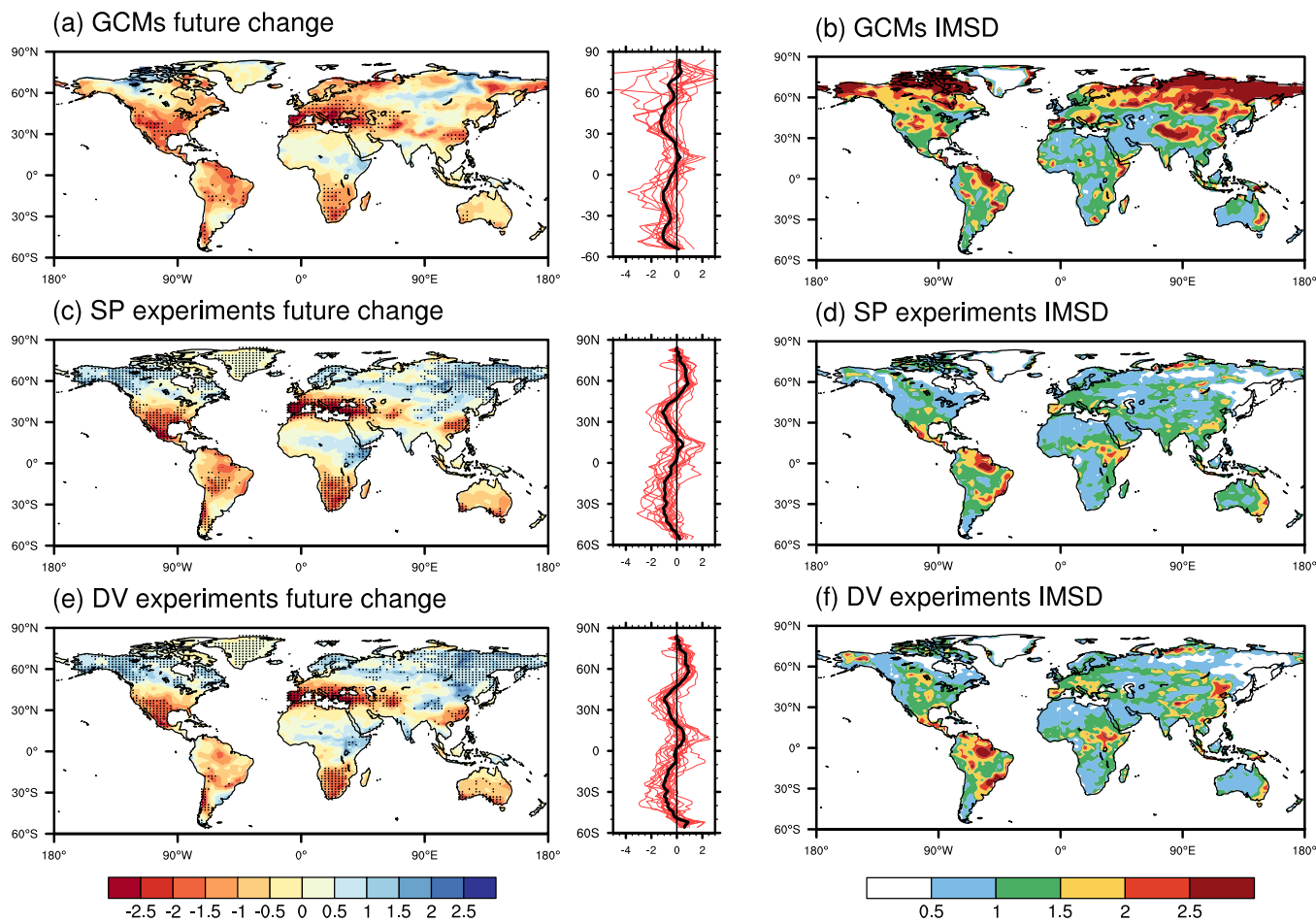


**Figure 9.** Similar as Figure 5, but for soil water in top 10cm (unit:  $\text{kg}/\text{m}^3$ ). Stippled means 16/17 GCMs (exclude CMCC-CM & CNRM-CM5), or 17/19 SP or DV simulations agree on the sign of the change.

treating soil hydrology and likely snow hydrology/snowmelt there (Figure 10a). The zonal-averaged future changes in soil water content produced by the DV experiments show very similar pattern compared to that from the SP experiments, suggesting the limited effect caused by the dynamic vegetation on future change of shallow soil water content. The amplification effect due to dynamic vegetation is large in some areas of North America, the southern Amazon, the Congo Basin, the Tibetan Plateau and about 50–60°N of Central and East Asia (Figure 10b).

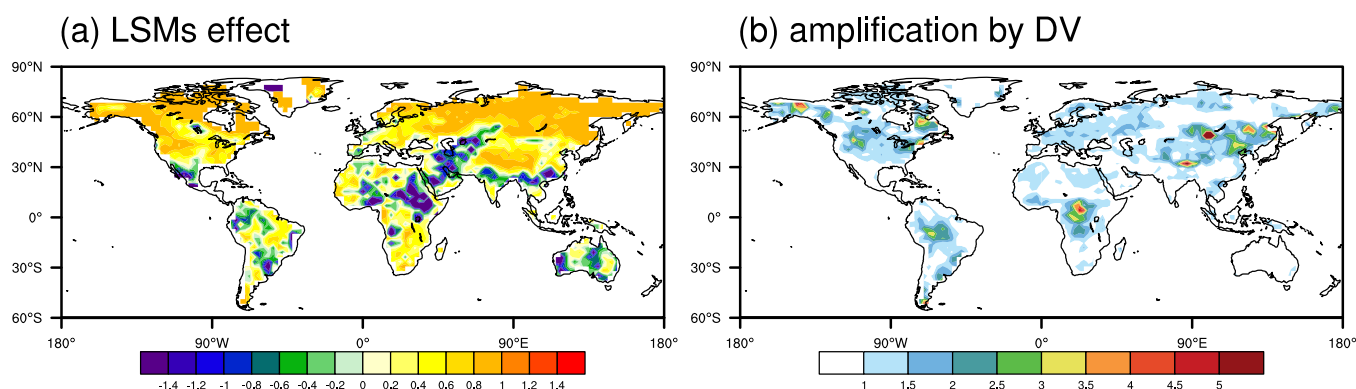


**Figure 10.** Similar as Figure 6, but for soil water in top 10 cm.

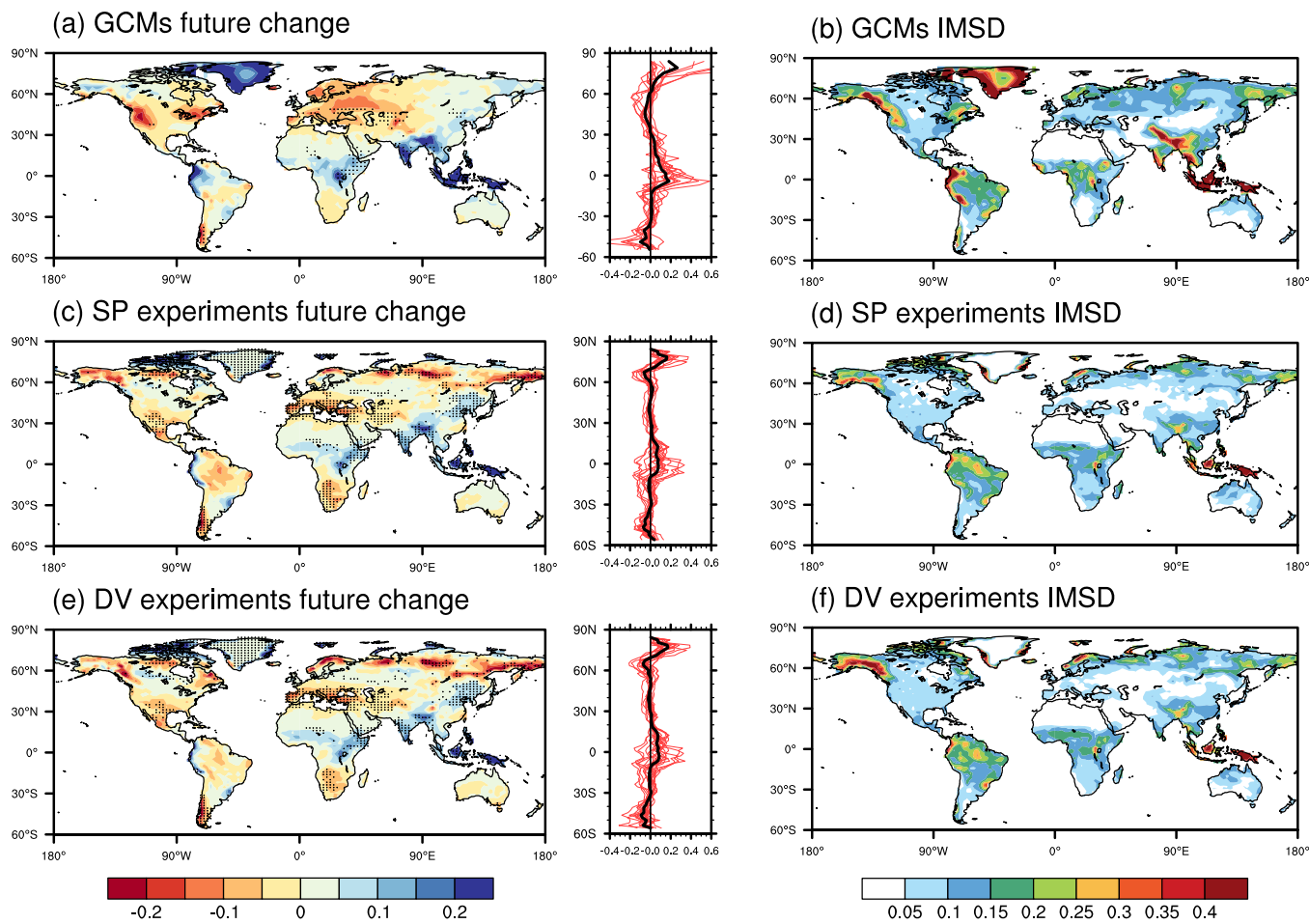


**Figure 11.** Similar as Figure 5, but for surface runoff (unit: mm/d). Stippled means 16/17 GCMs (exclude CMCC-CM & HadGEM-ES), or 17/19 SP or DV simulations agree on the sign of the change.

The SP and DV experiments produce very similar patterns of future surface runoff changes, suggesting a limited effect of dynamic vegetation on surface runoff (Figure 11). The intermodel uncertainty is amplified by dynamic vegetation in the moist areas of the Amazon and Central Africa, and the northern high latitudes including western and eastern Canada and about 50–60°N of Eurasia. In the arid areas of North Africa and the Arabian Peninsula, the extremely large value may not show a real influence of the dynamic vegetation,

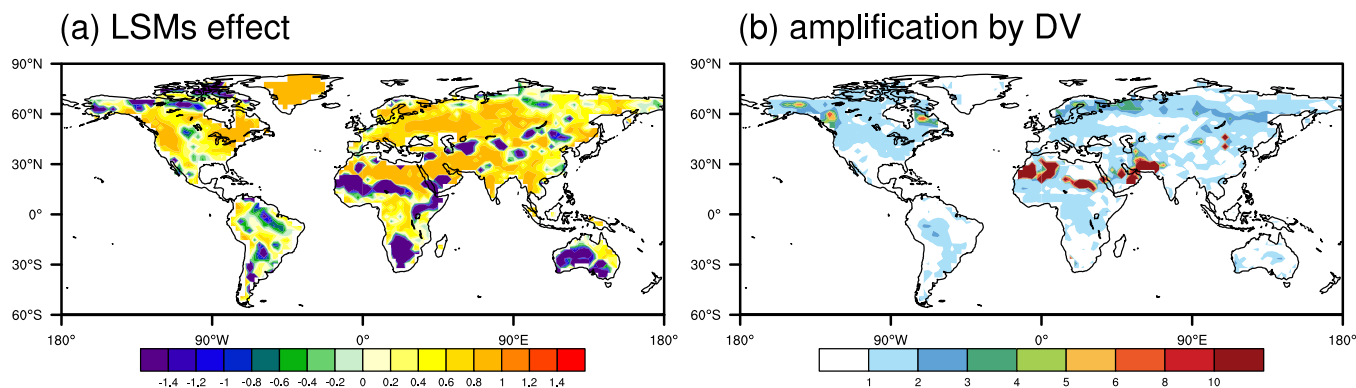


**Figure 12.** Similar as Figure 6, but for surface runoff.

because there is little runoff or vegetation and the intermodel spread is very small, resulting in large values for the ratio of two small variances there (Figure 12b). The GCMs project a large increase of surface runoff in Greenland and South Asia, and a decrease in northwestern U.S. and areas around the Great Lakes. But large intermodel spread exists in these areas.

#### 4. Summary and Discussion

To investigate the sources of uncertainties in the simulated future changes of surface water and energy fluxes, output from 19 GCMs participating in the CMIP5 are compared to output from offline experiments that use a modified version of CLM4 driven with atmospheric forcing from the 19 GCMs. The impact of dynamic vegetation on the uncertainties is investigated based on another group of experiments using CLM4-CNDV, the land surface model with the dynamic vegetation component, driven with the atmospheric forcing from the same 19GCMs. The intermodel agreement and the IMSD are used to provide quantified estimates of uncertainties caused by LSM schemes and to assess the influence of dynamic vegetation based on the annual average of projected future changes.

Under RCP8.5, results from the 19 GCMs support the consensus that global temperature will increase by more than 2°C with the northern high latitudes enduring the most severe warming trend. The IMSD for projected temperature changes is relatively small compared to that in the boreal region. Precipitation is projected to decrease in the areas around the Mediterranean, southwestern North America, most of South America, and South Africa, and increase in the area north of 50°N, south Asia, and the maritime subcontinent. Large uncertainties for the simulated future change of precipitation mainly are found in the Tropics. These uncertainties, together with uncertainties in the changes of other surface meteorological forcing as well as intermodel variation of land surface schemes, contribute to uncertainties in the projected changes of surface energy and water budgets.

Results from experiments using CLM4 driven with surface meteorological forcing from different GCMs indicate that the LSMs are important source of uncertainties contributing to the model dependency of the projected surface flux changes. LSMs' contribution to uncertainties in projected ET changes is significant in a large area north of about 40°N in Europe, Central Asia, and the northern North America. Their contribution to uncertainties of projected sensible heat flux changes is important in the Greenland, Central part of North Asia, and the Amazon. Contribution from LSMs to future change uncertainties is large for soil water content in the top 10 cm in the northern high latitudes and the Tibetan Plateau, and for the surface runoff primarily in the arid area, such as the western North America, North Africa, and West and Central Asia. As explained in section 2.4, these results are subject to uncertainties due to the difficulty to exclude internal variability from the intermodel spread and the complicating effect due to the lack of feedback from land surface to atmosphere in the offline CLM experiments.

Including dynamic vegetation is expected to enhance the uncertainties of the projected changes of annual means in surface fluxes and conditions, with stronger impact on changes in sensible heat flux than in ET, soil water content and surface runoff. Among the regions that are highly sensitive to vegetation dynamics are areas over about 50–70°N of Central and East Asia, the northwestern North America and the Amazon where the projected LAI future changes are subject to a large degree of uncertainties. The Tibetan Plateau is another region where large uncertainties for the projected future changes in vegetation and climate are found.

Results from this study have several important implications. First, the location of the strong LSMs contribution to the model dependency of projected changes in surface water and energy budgets (primarily in northern mid and high-latitudes) indicates that the largest intermodel variation in LSMs might have to do with how snow and soil ice processes are treated. These aspects of land surface modeling should be treated with high priority in future model development. As indicated earlier, due to the lack of important land-atmosphere coupling mechanisms, the offline modeling approach used here has several limitations. However, it does provide a starting point in demonstrating the potential to reduce the range of uncertainty in future projections by improving land surface models. To more realistically characterize the role of land surface processes including vegetation changes and their interactions with the rest of the climate system, it is desirable that future research make use of fully coupled simulations with transplanted land surface schemes [Wei *et al.*, 2010a; Wei *et al.*, 2010b]. Second, as dynamic vegetation models are being added to more earth

system models, future climate projections from the next generation models are likely subject to significantly higher degree of model dependency than those in CMIP3 and CMIP5. The strong impact of dynamic vegetation in enhancing the model uncertainties found in this study may be model-dependent. There is a need for further research to conduct similar experiments using other dynamic vegetation models to verify findings from this study. Meanwhile, given the potentially strong impact of including dynamic vegetation on model uncertainties, it is critical that we improve the accuracy of dynamic vegetation models and better understand the interactions between vegetation dynamics and the rest of the climate system.

#### Acknowledgments

Funding support for this study was provided by the U.S. National Science Foundation Climate and Large Scale Dynamics Program (AGS 1049017 and AGS 1063986), the National Natural Science Foundation of China (grant No. 41205084 and No. 41575084), and the Project Funded by the Priority Academic Program Development of Jiangsu Higher Education Institutions (PAPD). The authors are indebted to two anonymous reviewers whose constructive comments significantly improved the quality of this paper. We thank the World Climate Research Programme's Working Group on Coupled Modeling, which is responsible for CMIP. We also thank the climate modeling groups listed in Table 1 of this paper for producing and making their model output available. For CMIP, the US Department of Energy's Program for Climate Diagnosis and Intercomparison provides coordinating support and led development of software infrastructure in partnership with the Global Organization for Earth System Science Portals. All the CMIP5 model output is obtained through <http://cmip-pcmdi.llnl.gov/cmip5/availability.html>.

#### References

- Ahlström, A., B. Smith, J. Lindström, M. Rummukainen, and C. Uvo (2013), GCM characteristics explain the majority of uncertainty in projected 21st century terrestrial ecosystem carbon balance, *Biogeosciences*, 10(3), 1517–1528.
- Alessandri, A., P. G. Fogli, M. Vichi, and N. Zeng (2012), Strengthening of the hydrological cycle in future scenarios: Atmospheric energy and water balance perspective, *Earth Syst. Dyn. Discuss.*, 3(2), 199–212.
- Barnett, T. P., D. W. Pierce, H. G. Hidalgo, C. Bonfils, B. D. Santer, T. Das, G. Bala, A. W. Wood, T. Nozawa, and A. A. Mirin (2008), Human-induced changes in the hydrology of the western United States, *Science*, 319(5866), 1080–1083.
- Bellucci, A., S. Gualdi, S. Masina, A. Storto, E. Scoccimarro, C. Cagnazzo, P. Fogli, E. Manzini, and A. Navarra (2013), Decadal climate predictions with a coupled OGCM initialized with oceanic reanalyses, *Clim. Dyn.*, 40(5–6), 1483–1497.
- Bi, D., M. Dix, S. Marsi, S. O'Farrell, H. Rashid, P. Uotila, A. Hirst, E. Kowalczyk, M. Golebiewski, and A. Sullivan (2013), The ACCESS coupled model: Description, control climate and evaluation, *Aust. Meteorol. Oceanogr. J.*, 63, 9–32.
- Bonan, G. B. (2008), Forests and climate change: Forcings, feedbacks, and the climate benefits of forests, *Science*, 320, 1444–1449.
- Collins, M., et al. (2013), Long-term climate change: Projections, commitments and irreversibility, in *Climate Change 2013: The Physical Science Basis. Contribution of Working Group I to the Fifth Assessment Report of the Intergovernmental Panel on Climate Change*, edited by T. F. Stocker et al., pp.1029–1136, Cambridge University Press, Cambridge, U. K.
- Collins, W. J., et al. (2011), Development and evaluation of an Earth-system model: HadGEM2, *Geosci. Model Dev. Discuss.*, 4(2), 997–1062.
- Cox, P. M. (2001), Description of the TRIFFID dynamic global vegetation model, *Tech. Note 24*, Hadley Cent., U. K. Meteorol. Off., Bracknell, U. K.
- Dai, A. (2013), Increasing drought under global warming in observations and models, *Nat. Clim. Change*, 3(1), 52–58.
- Deser, C., A. Phillips, V. Bourdette, and H. Teng (2012), Uncertainty in climate change projections: The role of internal variability, *Clim. Dyn.*, 38(3–4), 527–546.
- Donner, L. J., et al. (2011), The dynamical core, physical parameterizations, and basic simulation characteristics of the atmospheric component AM3 of the GFDL global coupled model CM3, *J. Clim.*, 24(13), 3484–3519.
- Dufresne, J.-L., et al. (2013), Climate change projections using the IPSL-CM5 Earth System Model: From CMIP3 to CMIP5, *Clim. Dyn.*, 40(9), 2123–2165.
- Dunne, J. P., et al. (2012), GFDL's ESM2 global coupled climate–carbon earth system models. Part I: Physical formulation and baseline simulation characteristics, *J. Clim.*, 25(19), 6646–6665.
- Friedlingstein, P., P. Cox, R. Betts, L. Bopp, W. Von Bloh, V. Brovkin, P. Cadule, S. Doney, M. Eby, and I. Fung (2006), Climate–carbon cycle feedback analysis: Results from the C4MIP model intercomparison, *J. Clim.*, 19(14), 3337–3353.
- Gent, P. R., G. Danabasoglu, L. J. Donner, M. M. Holland, E. C. Hunke, S. R. Jayne, D. M. Lawrence, R. B. Neale, P. J. Rasch, and M. Vertenstein (2011), The community climate system model version 4, *J. Clim.*, 24(19), 4973–4991.
- Gotangco Castillo, C. K., S. Levis, and P. Thornton (2012), Evaluation of the new CNVD option of the community land model: Effects of dynamic vegetation and interactive nitrogen on CLM4 means and variability, *J. Clim.*, 25(11), 3702–3714.
- Griffies, S. M., et al. (2011), The GFDL CM3 coupled climate model: Characteristics of the ocean and sea ice simulations, *J. Clim.*, 24(13), 3520–3544.
- Hawkins, E., and R. Sutton (2009), The potential to narrow uncertainty in regional climate predictions, *Bull. Am. Meteorol. Soc.*, 90(8), 1095–1107.
- Hawkins, E., and R. Sutton (2011), The potential to narrow uncertainty in projections of regional precipitation change, *Clim. Dyn.*, 37(1–2), 407–418.
- Higgins, P. A., and J. Harte (2012), Carbon cycle uncertainty increases climate change risks and mitigation challenges, *J. Clim.*, 25(21), 7660–7668.
- Hosaka, M. (2011), *A new MRI land surface model HAL*, paper presented at AGU Fall Meeting Abstracts.
- Hua, W., H. Chen, S. Zhu, S. Sun, M. Yu, and L. Zhou (2013), Hotspots of the sensitivity of the land surface hydrological cycle to climate change, *Chin. Sci. Bull.*, 58(30), 3682–3688.
- Hurtt, G., S. Frolking, M. Fearon, B. Moore, E. Sheviakova, S. Malyshev, S. Pacala, and R. Houghton (2006), The underpinnings of land-use history: Three centuries of global gridded land-use transitions, wood-harvest activity, and resulting secondary lands, *Global Change Biol.*, 12(7), 1208–1229.
- Hurtt, G., L. P. Chini, S. Frolking, R. Betts, J. Feddema, G. Fischer, J. Fisk, K. Hibbard, R. Houghton, and A. Janetos (2011), Harmonization of land-use scenarios for the period 1500–2100: 600 years of global gridded annual land-use transitions, wood harvest, and resulting secondary lands, *Clim. Change*, 109(1–2), 117–161.
- IPCC AR4 (2007), Climate change 2007: The physical science basis, in *Contribution of working group I to the forth assessment report of the Intergovernmental Panel on Climate Change*, edited by S. Solomon et al., 996 pp., Cambridge Univ. Press, Cambridge.
- Ji, D., et al. (2014), Description and basic evaluation of BNU-ESM version 1, *Geosci. Model Dev. Discuss.*, 7(2), 1601–1647.
- Ji, J. (1995), A climate-vegetation interaction model: Simulating physical and biological processes at the surface, *J. Biogeogr.*, 22, 445–451.
- Ji, J., M. Huang, and K. Li (2008), Prediction of carbon exchanges between China terrestrial ecosystem and atmosphere in 21st century, *Sci. China Ser. D*, 51(6), 885–898.
- Jiang, Y., Q. Zhuang, S. Schaphoff, S. Sitch, A. Sokolov, D. Kicklighter, and J. Melillo (2012), Uncertainty analysis of vegetation distribution in the northern high latitudes during the 21st century with a dynamic vegetation model, *Ecol. Evol.*, 2(3), 593–614.
- Kay, J. E., et al. (2014), The Community Earth System Model (CESM) Large ensemble project: A community resource for studying climate change in the presence of internal climate variability, *Bull. Am. Meteorol. Soc.*, 96(8), 1333–1349.

- Knutti, R., and J. Sedláček (2013), Robustness and uncertainties in the new CMIP5 climate model projections, *Nat. Clim. Change*, 3(4), 369–373.
- Knutti, R., R. Furrer, C. Tebaldi, J. Cermak, and G. A. Meehl (2010), Challenges in combining projections from multiple climate models, *J. Clim.*, 23(10), 2739–2758.
- Lawrence, D. M., et al. (2011), Parameterization improvements and functional and structural advances in Version 4 of the Community Land Model, *J. Adv. Model. Earth Syst.*, 3, M03001, doi:10.1029/2011MS00045.
- Levis, S., G. B. Bonan, M. Vertenstein, and K. W. Oleson (2004), The community land model's dynamic global vegetation model (CLM-DGVM): Technical description and user's guide, *Rep. NCAR/TN-459+IA*, 50 pp., Nat. Cent. Atmos. Res., Boulder, Colo.
- Li, L., P. Lin, Y. Yu, B. Wang, T. Zhou, L. Liu, J. Liu, Q. Bao, S. Xu, and W. Huang (2013), The flexible global ocean-atmosphere-land system model, Grid-point Version 2: FGOALS-g2, *Adv. Atmos. Sci.*, 30, 543–560.
- Liang, X., and J. Guo (2003), Intercomparison of land-surface parameterization schemes: Sensitivity of surface energy and water fluxes to model parameters, *J. Hydrol.*, 279(1), 182–209.
- Mao, J., P. E. Thornton, X. Shi, M. Zhao, and W. M. Post (2012), Remote sensing evaluation of CLM4 GPP for the period 2000–09, *J. Clim.*, 25(15), 5327–5342.
- Martin, G., and R. Levine (2012), The influence of dynamic vegetation on the present-day simulation and future projections of the South Asian summer monsoon in the HadGEM2 family, *Earth Syst. Dyn. Discuss.*, 3(2), 759–799.
- Martin, G., M. Ringer, V. Pope, A. Jones, C. Dearden, and T. Hinton (2006), The physical properties of the atmosphere in the new Hadley Centre Global Environmental Model (HadGEM1). Part I: Model description and global climatology, *J. Clim.*, 19(7), 1274–1301.
- Moss, R. H., J. A. Edmonds, K. A. Hibbard, M. R. Manning, S. K. Rose, D. P. van Vuuren, T. R. Carter, S. Emori, M. Kainuma, and T. Kram (2010), The next generation of scenarios for climate change research and assessment, *Nature*, 463(7282), 747–756.
- Murphy, J. M., D. M. Sexton, D. N. Barnett, G. S. Jones, M. J. Webb, M. Collins, and D. A. Stainforth (2004), Quantification of modelling uncertainties in a large ensemble of climate change simulations, *Nature*, 430(7001), 768–772.
- Murray-Tortarolo, G., et al. (2013), Evaluation of land surface models in reproducing satellite-derived LAI over the high-latitude northern hemisphere. Part I: Uncoupled DGVMs, *Remote Sens.*, 5(10), 4819–4838.
- O'Gorman, P., and C. Muller (2010), How closely do changes in surface and column water vapor follow Clausius–Clapeyron scaling in climate change simulations?, *Environ. Res. Lett.*, 5(2), 025207.
- Oleson, K. W., et al. (2008), Improvements to the community land model and their impact on the hydrological cycle, *J. Geophys. Res.*, 113, G01021, doi:10.1029/2007JG000563.
- Oleson, K. W., et al. (2010), Technical description of version 4.0 of the Community Land Model (CLM), *Rep. NCAR/TN-478+STR*, 257 pp., Nat. Cent. Atmos. Res., Boulder, Colo.
- Piao, S., et al. (2012), The carbon budget of terrestrial ecosystems in East Asia over the last two decades, *Biogeosciences*, 9, 3571–3586.
- Pitman, A. J., and A. Henderson-Sellers (1998), Recent progress and results from the project for the intercomparison of landsurface parameterization schemes, *J. Hydrol.*, 212(1–4), 128–135.
- Roberts, J. M., O. M. R. Cabral, J. P. Costa, A. L. C. McWilliam, and T. D. A. Sa (1996), *An Overview of the Leaf Area Index and Physiological Measurement During ABRACOS*, John Wiley, Chichester, N. Y.
- Shao, P., X. Zeng, K. Sakaguchi, R. K. Monson, and X. Zeng (2013), Terrestrial carbon cycle: Climate relations in eight CMIP5 Earth System Models, *J. Clim.*, 26(22), 8744–8764.
- Sheviakova, E., S. W. Pacala, S. Malyshev, G. C. Hurtt, P. C. D. Milly, J. P. Caspersen, L. T. Sentman, J. P. Fisk, C. Wirth, and C. Crevoisier (2009), Carbon cycling under 300 years of land use change: Importance of the secondary vegetation sink, *Global Biogeochem. Cycles*, 23, GB2022, doi:10.1029/2007GB003176.
- Stockli, R., D. M. Lawrence, G.-Y. Niu, K. W. Oleson, P. E. Thornton, Z.-L. Yang, G. B. Bonan, A. S. Denning, and S. W. Running (2008), Use of FLUXNET in the Community Land Model development, *J. Geophys. Res.*, 113, G01025, doi:10.1029/2007JG000562.
- Takata, K., S. Emori, and T. Watanabe (2003), Development of the minimal advanced treatments of surface interaction and runoff, *Global Planet. Change*, 38(1), 209–222.
- Taylor, K. E., R. J. Stouffer, and G. A. Meehl (2012), An overview of CMIP5 and the experiment design, *Bull. Am. Meteorol. Soc.*, 93(4), 485–498.
- Thornton, P. E., and N. A. Rosenbloom (2005), Ecosystem model spin-up: Estimating steady state conditions in a coupled terrestrial carbon and nitrogen cycle model, *Ecol. Model.*, 189(1), 25–48.
- Thornton, P. E., B. Law, H. L. Gholz, K. L. Clark, E. Falge, D. Ellsworth, A. Goldstein, R. Monson, D. Hollinger, and M. Falk (2002), Modeling and measuring the effects of disturbance history and climate on carbon and water budgets in evergreen needleleaf forests, *Agric. For. Meteorol.*, 113(1), 185–222.
- Thornton, P. E., J.-F. Lamarque, N. A. Rosenbloom, and N. M. Mahowald (2007), Influence of carbon-nitrogen cycle coupling on land model response to CO<sub>2</sub> fertilization and climate variability, *Global Biogeochem. Cycles*, 21, GB4018, doi:10.1029/2006GB002868.
- Tucker, C. J., J. E. Pinzon, M. E. Brown, D. A. Slayback, E. W. Pak, R. Mahoney, E. F. Vermote, and N. E. Saleous (2005), An extended AVHRR 8-km NDVI dataset compatible with MODIS and SPOT vegetation NDVI data, *Int. J. Remote Sens.*, 26(20), 4485–4498.
- Voldoire, A., et al. (2013), The CNRM-CM5.1 global climate model: Description and basic evaluation, *Clim. Dyn.*, 40(9), 2091–2121.
- Volodin, E., and V. Lykosov (1998), Parametrization of heat and moisture transfer in the soil-vegetation system for use in atmospheric general circulation models: 1. Formulation and simulations based on local observational data, *Izv. Atmos. Oceanic Phys.*, 34(4), 405–416.
- Volodin, E., N. Dianskii, and A. Gusev (2010), Simulating present-day climate with the INMCM4.0 coupled model of the atmospheric and oceanic general circulations, *Izv. Atmos. Oceanic Phys.*, 46(4), 414–431.
- Wang, G. (2005), Agricultural drought in a future climate: Results from 15 global climate models participating in the IPCC 4th assessment, *Clim. Dyn.*, 25(7–8), 739–753.
- Wang, G., M. Yu, J. S. Pal, R. Mei, G. B. Bonan, S. Levis, and P. Thornton (2015), On the development of a coupled regional climate-vegetation model RCM-CLM-CN-DV and its validation in Tropical Africa, *Clim. Dyn.*, doi:10.1007/s00382-015-2596-z.
- Watanabe, M., T. Suzuki, R. Oishi, Y. Komuro, S. Watanabe, S. Emori, T. Takemura, M. Chikira, T. Ogura, and M. Sekiguchi (2010), Improved climate simulation by MIROC5: Mean states, variability, and climate sensitivity, *J. Clim.*, 23(23), 6312–6335.
- Watanabe, S., et al. (2011), MIROC-ESM 2010: Model description and basic results of CMIP5-20c3m experiments, *Geosci. Model Dev.*, 4(4), 845–872.
- Wei, J., P. A. Dirmeyer, and Z. Guo (2010a), How much do different land models matter for climate simulation? Part II: A decomposed view of the land–atmosphere coupling strength, *J. Clim.*, 23(11), 3135–3145.
- Wei, J., P. A. Dirmeyer, Z. Guo, L. Zhang, and V. Misra (2010b), How much do different land models matter for climate simulation? Part I: Climatology and variability, *J. Clim.*, 23(11), 3120–3134.

- Wood, E. F., et al. (1998), The Project for Intercomparison of Land-surface Parameterization Schemes (PILPS) phase 2(c) Red-Arkansas River basin experiment: 1. Experiment description and summary intercomparisons, *Global Planet. Change*, 19(1–4), 115–135.
- Wu, T., W. Li, J. Ji, X. Xin, L. Li, Z. Wang, Y. Zhang, J. Li, F. Zhang, and M. Wei (2013), Global carbon budgets simulated by the Beijing Climate Center Climate System Model for the last century, *J. Geophys. Res. Atmos.*, 118, 4326–4347, doi:10.1002/jgrd.50320.
- Wu, T., et al. (2014), An overview of BCC climate system model development and application for climate change studies, *Acta Meteorol. Sin.*, 28(1), 34–56.
- Yu, M., G. Wang, D. Parr, and K. F. Ahmed (2014), Future changes of the terrestrial ecosystem based on a dynamic vegetation model driven with RCP8.5 climate projections from 19 GCMs, *Clim. Change*, 127(2), 257–271.
- Yu, M., G. Wang, and J. S. Pal (2015), Effects of vegetation feedback on future climate change over Tropical Africa, *Clim. Dyn.*, in press.
- Yukimoto, S., Y. Adachi, and M. Hosaka (2012), A new global climate model of the Meteorological Research Institute: MRI-CGCM3: Model description and basic performance (special issue on recent development on climate models and future climate projections), *J. Meteorol. Soc. Jpn.*, 90, 23–64.
- Zhou, L., C. J. Tucker, R. K. Kaufmann, and E. Al (2001), Variations in Northern vegetation activity inferred from satellite data of vegetation index during 1981 to 1999, *J. Geophys. Res.*, 106, 20,069–20,083.